J|A|C|S
ARTICLES

Published on Web 02/04/2010

Anthracene−BODIPY Dyads as Fluorescent Sensors for Biocatalytic Diels−Alder Reactions

Alexander Nierth,[†] Andrei Yu. Kobitski,[‡] G. Ulrich Nienhaus,[‡,§] and Andres Jäschke*[,†]

Institute of Pharmacy and Molecular Biotechnology, Heidelberg University, Im Neuenheimer Feld 364, Heidelberg 69120, Germany, Institute of Applied Physics and Center for Functional Nanostructures, Karlsruhe Institute of Technology, Wolfgang-Gaede-Strasse 1, 76131 Karlsruhe, Germany, and Department of Physics, University of Illinois at Urbana−Champaign, Urbana, Illinois 61801

Received October 4, 2009; E-mail: jaeschke@uni-hd.de

Abstract: Fluorescence spectroscopy is a powerful, extremely sensitive technique for the investigation of enzyme and ribozyme mechanisms. Herein, we describe the synthesis and characterization of water-soluble fluorescence probes for studying biocatalytic Diels−Alder reactions. These probes consist of anthracene and sulfonated BODIPY fluorophores fused by conjugated phenylacetylenyl bridges. Intact anthracene efficiently quenches BODIPY fluorescence, likely by photoinduced electron transfer. Upon destruction of the aromatic system by the Diels−Alder reaction, the fluorescence emission increases 20-fold. Binding in the catalytic pocket of a Diels−Alderase ribozyme yields a further ∼2-fold increase in the fluorescence intensity of both the anthracene−BODIPY and the Diels−Alder-product−BODIPY probes. Therefore, a fluorescence-based distinction of free substrate, bound substrate, bound product, and free product is possible. With these all-in-one reporters, we monitored RNA-catalyzed Diels−Alder reactions under both single- and multiple-turnover conditions down to the nanomolar concentration range. Burst analysis at the single-molecule level revealed blinking of the dyads between an on state and an off state, presumably due to rotation around the phenylacetylenyl bridge. Binding to the ribozyme does not increase the intensity of the individual fluorescence bursts, but rather increases the average time spent in the on state. Variations in the quantum yields of the different probes correlate well with the degree of conjugation between anthracene and the phenylacetylenyl bridge.

Introduction

Fluorescent reporter molecules have become indispensable tools in all areas of science and have contributed significantly to our understanding of chemical and biological systems. Ideally, the fluorescence emission properties of the sensor change upon binding, reaction, or environmental changes in a characteristic manner, thereby generating an optical output signal. Different chemosensors have been developed that are sensitive to pH,[1,2] solvent polarity,[3] heavy-metal ions,[4] and small molecules.[5] In biology, fluorescent probes enable a vast range of experimental techniques, from live cell imaging to mechanistic studies at the single-molecule level.[6−8]

Fluorescent probes have also permitted investigations of the catalytic mechanisms of various enzymes.[9,10] Ideally, the probe's fluorescence properties should allow one to distinguish between free substrate, bound substrate, bound product, and free product to observe the fundamental species of a catalytic cycle. Progress in single-molecule enzymology is, however, restricted by the paucity of substrate-analogue probes with suitable properties.[11] Whereas fluorescence labeling is frequently straightforward for macromolecular substrates of enzymes such as proteases or nucleases, it is challenging or even entirely impossible for many small-molecule substrates.

Our laboratory has a long-standing interest in catalysis by ribonucleic acids (ribozymes). We have discovered—by combinatorial chemistry—ribozymes that catalyze C−C bond formation by Diels−Alder reaction between two small-molecule substrates, namely, anthracenes as dienes and *N*-substituted maleimides as dienophiles (Figure 1A).[12] These ribozymes show multiple turnovers and saturation behavior and have been

[†] Heidelberg University.
[‡] Karlsruhe Institute of Technology.
[§] University of Illinois at Urbana−Champaign.

(1) Han, J.; Loudet, A.; Barhoumi, R.; Burghardt, R. C.; Burgess, K. *J. Am. Chem. Soc.* **2009**, *131*, 1642–1643.
(2) Baruah, M.; Qin, W. W.; Basaric, N.; De Borggraeve, W. M.; Boens, N. *J. Org. Chem.* **2005**, *70*, 4152–4157.
(3) Sunahara, H.; Urano, Y.; Kojima, H.; Nagano, T. *J. Am. Chem. Soc.* **2007**, *129*, 5597–5604.
(4) Komatsu, K.; Urano, Y.; Kojima, H.; Nagano, T. *J. Am. Chem. Soc.* **2007**, *129*, 13447–13454.
(5) Gabe, Y.; Urano, Y.; Kikuchi, K.; Kojima, H.; Nagano, T. *J. Am. Chem. Soc.* **2004**, *126*, 3357–3367.
(6) Eid, J.; et al. *Science* **2009**, *323*, 133–138.
(7) Nienhaus, G. U. *Angew. Chem., Int. Ed.* **2008**, *47*, 8992–8994.
(8) Röcker, C.; Pötzl, M.; Zhang, F.; Parak, W. J.; Nienhaus, G. U. *Nat. Nanotechnol.* **2009**, *4*, 577–580.
(9) Chen, Q.; Groote, R.; Schonherr, H.; Vancso, G. J. *Chem. Soc. Rev.* **2009**, *38*, 2671–2683.
(10) Smiley, R. D.; Hammes, G. G. *Chem. Rev.* **2006**, *106*, 3080–3094.
(11) Jung, G.; Schmitt, A.; Jacob, M.; Hinkeldey, B. *Ann. N.Y. Acad. Sci.* **2008**, *1130*, 131–137.
(12) Seelig, B.; Jäschke, A. *Chem. Biol.* **1999**, *6*, 167–176.

 10.1021/ja9084397

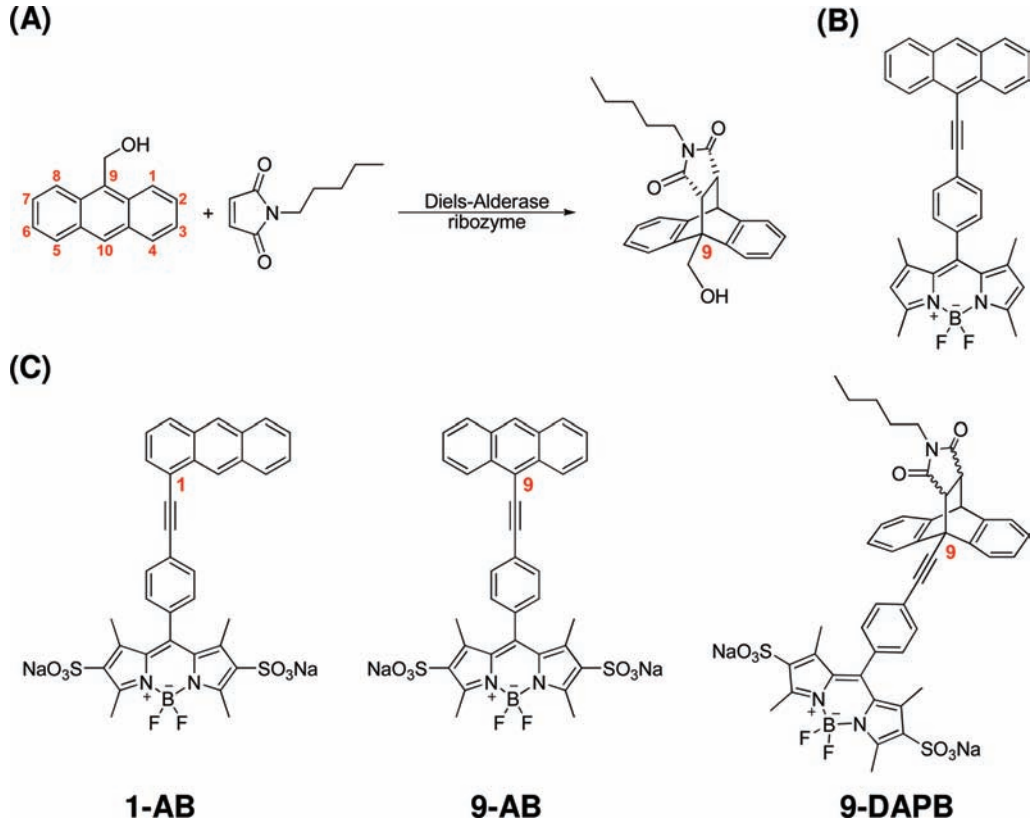

Figure 1. (A) Ribozyme-catalyzed Diels−Alder reaction between 9-hydroxymethylanthracene and *N*-pentylmaleimide.[15] (B) Energy-transfer cassette developed by the Burgess laboratory.[23] (C) Design of sensors for the investigation of Diels−Alder reactions: substrate-analogue probes 1-AB, 9-AB, and product-analogue probe 9-DAPB.

investigated by using numerous crystallographic, spectroscopic, computational, chemical, and biochemical techniques.[13−18] Despite all of these efforts, both the exact kinetic scheme and the catalytic mechanism of ribozyme-catalyzed Diels−Alder reactions are presently still unknown. There have been numerous proposals,[16,19,20] but clear evidence has been evasive.

Measurements of the reaction rates and kinetic constants have so far been based on the intrinsic absorption and fluorescence properties of the anthracene substrate. Upon Diels−Alder reaction, the conjugated π-system of anthracene is destroyed, and the reduction of anthracene fluorescence directly reports the consumption of anthracene. The product can, however, no longer be observed because it is nonfluorescent, and there is also no significant difference in the fluorescence emission between free and bound anthracene substrate. Moreover, an excitation wavelength below 370 nm precludes the extension of our previous single-molecule folding studies on this ribozyme[21] to substrate binding and catalysis, as current single-molecule fluorescence experiments require highly fluorescent probes, with excitation and emission wavelengths above 400 nm.

We therefore started the development of fluorescent molecular probes for catalytic Diels−Alder reactions that satisfy the following criteria: (1) excitation and emission wavelengths above 400 nm; (2) sufficient solubility in aqueous solvent; (3) reactivity as a diene in (uncatalyzed) Diels−Alder reactions similar to the original substrate; (4) acceptance as a substrate by the ribozyme; and (5) fluorescent properties that are affected not only by the Diels−Alder reaction, but also by binding to the ribozyme, allowing different species of the catalytic cycle to be distinguished.

Preliminary attempts to connect anthracene to a second fluorophore via a flexible tether did not result in compounds that satisfied all of these criteria (data not shown). We reasoned that direct electronic communication between the two modules, for example, through a conjugated π-system, would be more promising to yield useful probes.[22] In this approach, we were inspired by the "energy-transfer cassettes" developed by Burgess and co-workers,[23] which are anthracenes and fluorophores fused by conjugated, unsaturated bridges (Figure 1B), thereby creating large virtual Stokes shifts. 4,4-Difluoro-1,3,5,7-tetramethyl-4-bora-3a,4a-diaza-*s*-indacene (BODIPY) combines many advantageous fluorescence characteristics, including high brightness

(13) Keiper, S.; Bebenroth, D.; Seelig, B.; Westhof, E.; Jäschke, A. *Chem. Biol.* **2004**, *11*, 1217–1227.
(14) Kisseleva, N.; Kraut, S.; Jäschke, A.; Schiemann, O. *HFSP J.* **2007**, *1*, 127–136.
(15) Seelig, B.; Keiper, S.; Stuhlmann, F.; Jäschke, A. *Angew. Chem., Int. Ed.* **2000**, *39*, 4576–4579.
(16) Serganov, A.; Keiper, S.; Malinina, L.; Tereshko, V.; Skripkin, E.; Höbartner, C.; Polonskaia, A.; Phan, A. T.; Wombacher, R.; Micura, R.; Dauter, Z.; Jäschke, A.; Patel, D. J. *Nat. Struct. Mol. Biol.* **2005**, *12*, 218–224.
(17) Stuhlmann, F.; Jäschke, A. *J. Am. Chem. Soc.* **2002**, *124*, 3238–3244.
(18) Wombacher, R.; Jäschke, A. *J. Am. Chem. Soc.* **2008**, *130*, 8594–8595.
(19) Kim, S. P.; Leach, A. G.; Houk, K. N. *J. Org. Chem.* **2002**, *67*, 4250–4260.
(20) Zhang, X.; Bruice, T. C. *J. Am. Chem. Soc.* **2007**, *129*, 1001–1007.
(21) Kobitski, A. Y.; Nierth, A.; Helm, M.; Jäschke, A.; Nienhaus, G. U. *Nucleic Acids Res.* **2007**, *35*, 2047–2059.
(22) Flamigni, L.; Talarico, A. M.; Ventura, B.; Rein, R.; Solladie, N. *Chem.—Eur. J.* **2006**, *12*, 701–712.
(23) Wan, C. W.; Burghart, A.; Chen, J.; Bergström, F.; Johansson, L. B. A.; Wolford, M. F.; Kim, T. G.; Topp, M. R.; Hochstrasser, R. M.; Burgess, K. *Chem.—Eur. J.* **2003**, *9*, 4430–4441.

Scheme 1. Synthesis of Building Blocks[a]

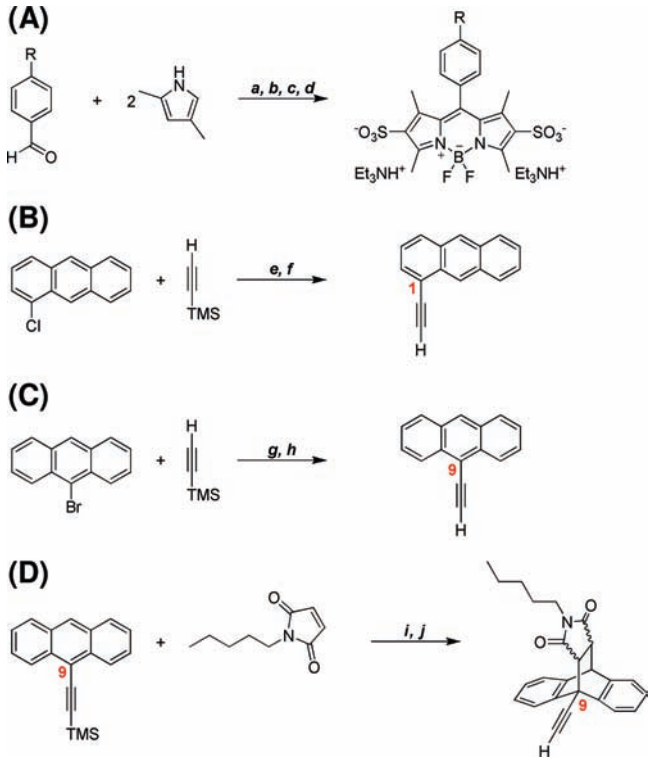

[a] Conditions: (A) a, catalytic TFA; b, DDQ; c, $BF_3 \cdot OEt_2$; d, $ClSO_3H$ and $NaHCO_3$ giving bromo-BODIPY (R = Br) and iodo-BODIPY (R = I). (B) e, EtMgBr, $Ni(acac)_2$ (acac = acetylacetonate), PPh_3. f, h, j, K_2CO_3, MeOH. (C) g, $Pd(PPh_3)_4$, CuI, DIPEA. (D) i, 115°C in toluene.

and quantum yield, sharp bands, and photostability.[24] This prior work laid the foundation for the design of our target compounds, in which anthracene and a BODIPY core are connected by a phenylacetylenyl bridge (Figure 1C). As the Burgess-type energy-transfer cassettes are not water-soluble, sulfonyl groups (the introduction of which into BODIPY derivatives is far from trivial[25]) were incorporated into the design. Two different anthracene positions were chosen as attachment points (positions 1 and 9) based on our knowledge on the effects of chemical substitutions on the acceptance as a substrate by the ribozyme,[17] leading to the probes anthracen-1-yl-BODIPY (1-AB) and anthracen-9-yl-BODIPY (9-AB). To establish the spectroscopic properties of the product resulting from the ribozyme-catalyzed reaction, a Diels−Alder product−BODIPY conjugate, 9-DAPB, was also designed.

Results and Discussion

Synthesis of Fluorescent Probes. The target compounds (Figure 1C) were synthesized following a convergent route. The halogenated and water-soluble BODIPY building block was accessible in four steps by a combination of literature procedures (Scheme 1A).[2,26,27] First, *p*-bromo- or *p*-iodobenzaldehyde was coupled with 2,4-dimethylpyrrole in a pyrrole condensation reaction using catalytic amounts of trifluoroacetic acid, followed by in situ oxidation with 2,3-dichloro-5,6-dicyano-*p*-benzoquinone (DDQ). The resulting dipyrromethene was complexed with boron trifluoride giving the fluorescent BODIPY core, which was then sulfonated using chlorosulfonic acid to yield the water-soluble derivatives (bromo-BODIPY and iodo-BODIPY). After purification by reverse-phase liquid chromatography, the highly fluorescent triethylammonium salts were obtained.

Anthracenes with alkyne linkers were obtained by transition-metal cross-coupling chemistry and trimethylsilane (TMS) protection (Scheme 1B,C). Whereas derivatization at the 1-position succeeded using Kumada−Corriu coupling with 1-chloroanthracene, the central 9-position could be converted most efficiently by Sonogashira−Hagihara-type reactions with 9-bromoanthracene. The TMS-protected 9-ethynylanthracene was also used for synthesis of the respective Diels−Alder product by thermal cycloaddition with *N*-pentylmaleimide (Scheme 1D). All TMS-protected alkynes were readily deprotected to the terminal alkynes using potassium carbonate and methanol.

The large difference in polarity and solubility of the two reacting components prevented the assembly of the final constructs under various combinations of "classical" reaction parameters (catalysts, bases, phase-transfer additives, solvents; data not shown).[28] Addition of the hydrophilic transition-metal ligand 3-(di-*tert*-butylphosphonium)propane sulfonate (DTBPPS)[29] led to appreciable product formation, and the best coupling results were obtained with 3.0 mol % $Pd(OAc)_2$, 3.0 mol % DTBPPS, 1.2 equiv of *N*,*N*-diisopropylethylamine (DIPEA), and 1.0 mol % of CuI as cocatalyst in mixtures of acetonitrile and water (Scheme 2). Using the bromo-functionalized BODIPY, 1-AB and 9-DAPB were obtained in good yields (46% and 51%), whereas for 9-AB, the higher reactivity of the iodo-BODIPY derivative was exploited (60% yield).

Purification by reverse-phase chromatography yielded the triethylammonium salts of the probes. To ensure purities of >99% in spectroscopic experiments, an additional purification by semipreparative reverse-phase high-performance liquid chromatography (HPLC) was conducted, followed by cation exchange to obtain the disodium salts.

For both anthracene derivatives, the fluorescence of the BODIPY moiety was found to be suppressed after reaction with the ethynylanthracene component, clearly visible by thin-layer chromatography (TLC) and HPLC, whereas structurally related compounds such as the Burgess-type energy-transfer cassettes or the free BODIPY-disulfonate are known to be highly fluorescent. The most likely explanation for this effect is a reductive photoinduced electron-transfer (PeT) process, which might arise because of the strong electron reduction potential of anthracene relative to the sulfonated BODIPY core.[3,25,30] Consequently, any change in the highest occupied molecular orbital/lowest unoccupied molecular orbital (HOMO/LUMO) energy levels of either anthracene or BODIPY should lead to an observable change in fluorescence intensity. Based on this assumption, we started a thorough spectroscopic investigation of the parameters that govern the fluorescence emission of these anthracene derivatives.

Spectroscopic Properties of the Free Probes. The absorption and fluorescence spectra of 1-AB, 9-AB, 9-DAPB, and reference compounds in aqueous Diels−Alderase (DAse) buffer [300 mM

(24) Loudet, A.; Burgess, K. *Chem. Rev.* **2007**, *107*, 4891–4932.
(25) Li, L. L.; Han, J. Y.; Nguyen, B.; Burgess, K. *J. Org. Chem.* **2008**, *73*, 1963–1970.
(26) Burghart, A.; Kim, H. J.; Welch, M. B.; Thoresen, L. H.; Reibenspies, J.; Burgess, K.; Bergström, F.; Johansson, L. B. A. *J. Org. Chem.* **1999**, *64*, 7813–7819.
(27) Chen, J.; Burghart, A.; Derecskei-Kovacs, A.; Burgess, K. *J. Org. Chem.* **2000**, *65*, 2900–2906.
(28) Chinchilla, R.; Najera, C. *Chem. Rev.* **2007**, *107*, 874–922.
(29) Brown, W. S.; Boykin, D. D.; Sonnier, M. Q.; Clark, W. D.; Brown, F. V.; Shaughnessy, K. H. *Synthesis* **2008**, 1965–1970.
(30) Heinis, T.; Chowdhury, S.; Kebarle, P. *Org. Mass Spectrom.* **1993**, *28*, 358–365.

Scheme 2. Final Coupling to Target Compounds 1-AB, 9-AB, and 9-DAPB

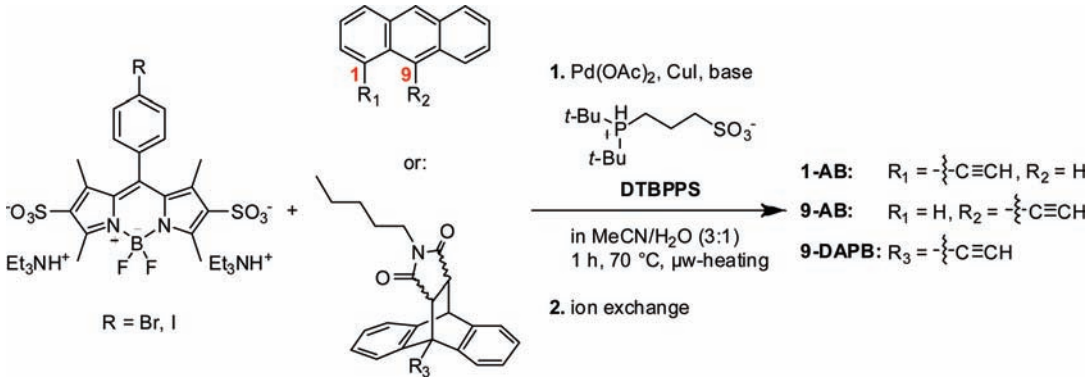

NaCl, 30 mM tris(hydroxymethyl)aminomethane hydrochloride (Tris·HCl), pH 7.4, 80 mM $MgCl_2$, and 10% ethanol] are shown in Figure 2; quantitative details are reported in Table 1.

The 1-AB and 9-AB spectra show characteristic features of both anthracene and BODIPY. All three new compounds have absorption maxima around 500 nm, ascribed to the BODIPY moiety, with only small differences in position and width (see also Figure S1A in the Supporting Information). Likewise, the secondary anthracene band at ~260 nm shows only slight shifts in wavelength. Major differences, compared to the reference

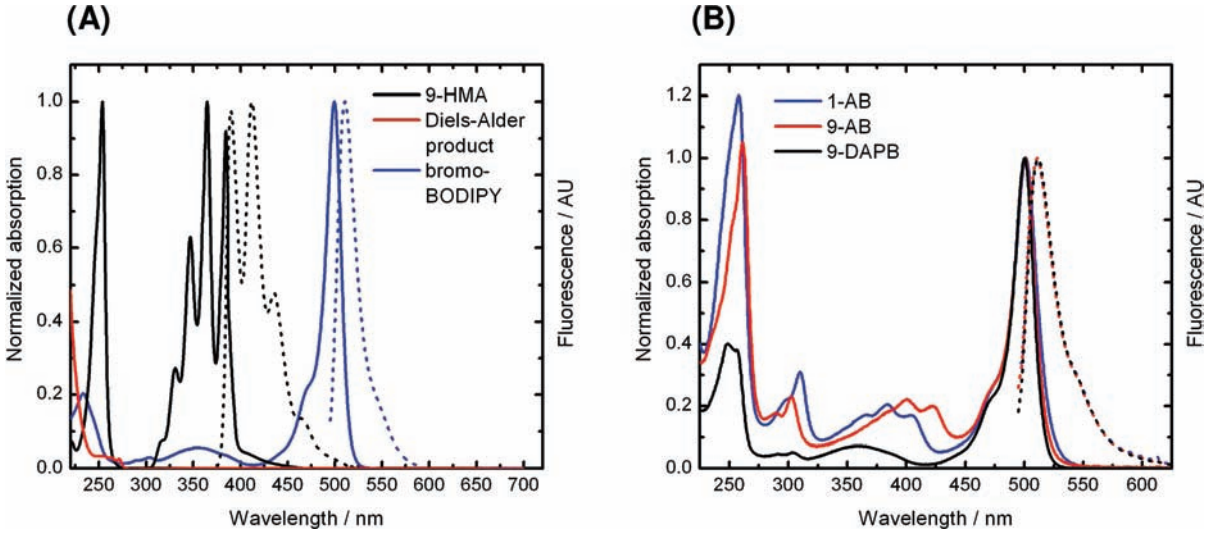

Figure 2. (A) Normalized absorption (solid lines) and fluorescence (dashed lines) spectra of reference compounds: 9-hydroxymethylanthracene (9-HMA, black, 10 μM at 220−300 nm, 100 μM at 300−450 nm, excited at 365 nm), respective Diels−Alder product (50 μM in ethanol, red, no observable fluorescence), and bromo-BODIPY (blue, absorption 10 μM, fluorescence 0.2 μM, excited at 488 nm). (B) Absorption (solid lines, 10 μM) and fluorescence (dashed lines, excited at 488 nm) spectra of 1-AB (blue, 100 μM), 9-AB (red, 100 μM), and 9-DAPB (black, 0.4 μM), normalized to the BODIPY absorption and emission maxima. All spectra were measured in standard DAse buffer, except the Diels−Alder product reference compound (panel A, red).

Table 1. Spectroscopic Properties of Sensors and Reference Compounds

	λ_{max}(abs)[a] (nm)					
compound	anthracene moiety	BODIPY moiety	λ_{max}(em)[b] (nm)	Φ[c]	r[d]	τ[e] (ns)
9-HMA	253, 315, 330, 346, 364, 384[f]	na[g]	390, 413, 437, 465[f]	nd[h]	nd[h]	5.47[i]
iodo-BODIPY disulfonate[25]	na[g]	498[j]	509[j]	0.34 ± 0.02[f]	nd[h]	2.1[j]
		499[f]	511[f]			2.0[f]
1-AB	257, 365, 384, 405[f]	499[j]	515[j]	0.006 ± 0.001[f]	0.10 ± 0.01[f]	1.5/4.5[j]
		501[f]	512[f]			1.4/2.5[f]
1-AB/RNA	na,[g] 367, 386, 407[f,m,n]	499[f,m,n]	514[f,m,n]	0.006[f,k]	0.16 ± 0.01[f,m,o]	1.3/3.5[f,m,o]
9-AB	261, 383, 400, 422[f]	499[j]	515[j]	0.014 ± 0.001[f]	0.05 ± 0.01[f]	2.4[j]
		501[f]	512[f]			2.4[f]
9-AB/RNA	na,[g] 386, 404, 426[f,m,o]	500[f,m,o]	513[f,m,o]	0.014[f,k]	0.11 ± 0.01[f,m,p]	2.5[f,m,p]
9-DAPB	(256), 325−400[f,l]	499[j]	510[j]	0.30 ± 0.03[f]	0.04 ± 0.01[f]	2.0[j]
		500[f]	512[f]			2.2[f]
9-DAPB/RNA	na,[g] 325−400[f,l,m,q]	499[f,m,q]	511[f,m,q]	0.42[f,k]	0.20 ± 0.01[f,m,q]	3.2[f,m,q]

[a] Absorption maxima. [b] Fluorescence emission maxima. [c] Quantum yield with respect to Rhodamine 6G (Φ = 0.95).[31] [d] Fluorescence emission anisotropy. [e] Fluorescence lifetime. [f] In standard DAse buffer (300 mM NaCl, 30 mM Tris·HCl, pH 7.4, 80 mM $MgCl_2$, and 10% ethanol). [g] Not applicable. [h] Not determined. [i] In ethanol. [j] In water. [k] Extrapolated quantum yield. [l] No fine structure. [m] Pocket occupancies determined from fluorescence correlation spectroscopy (FCS) data. [n] 60% bound. [o] 40% bound. [p] 50% bound. [q] 90% bound.

compounds, occur in the region of the lower $\pi \rightarrow \pi^*$ transitions (primary anthracene bands). The characteristic peaks of the anthracene core ("anthracene fingers" at 330, 346, 364, and 384 nm in standard DAse buffer) are considerably shifted to higher wavelengths for 1-AB and 9-AB.

The larger bathochromic shift in 9-AB (38 nm) than in 1-AB (21 nm) indicates a higher degree of conjugation between the anthracene and phenylacetylene components. The vibrational fine structure of these compounds is not lost in aqueous solution, indicating rather weak interactions with the solvent. As expected, conversion of the anthracene part to the Diels−Alder product strongly suppresses the electronic transitions below 450 nm as a result of destruction of the aromatic system.

Fluorescence emission spectra of all three compounds in standard DAse buffer show nearly identical locations of the emission maxima at 512 nm when excited at 488 nm, but largely different intensities. Sharp emission bands typical of the BODIPY fluorophore are observed; the quantum yields Φ are 0.006, 0.014, and 0.30 for 1-AB, 9-AB, and 9-DAPB, respectively. Apparently, the presence of the aromatic anthracene efficiently quenches the BODIPY fluorescence. In the Diels−Alder product, such quenching is much less efficient. The 20-fold difference in quantum yield between substrate and reaction product suggests that these probes could be quite suitable for monitoring Diels−Alder reactions.

To probe the anthracene−BODIPY interaction, emission spectra were also recorded with excitation at the (bathochromically shifted) anthracene absorbance maximum, 405 nm for 1-AB and 422 nm for 9-AB. Fluorescence emission occurred at 515 nm, although with a much lower intensity (see Figure S1B, Supporting Information). 9-DAPB exhibits very weak fluorescence under these conditions. The typical anthracene emission band ($\lambda_{max} = 413$ nm upon excitation at 260 or 364 nm) is not detectable in any of the compounds. Fluorescence excitation spectra for 1-AB and 9-AB differ from the corresponding absorption spectra in the spectral range of anthracene absorption (Figure S1C, Supporting Information) and resemble the absorption spectrum for 9-DAPB (Figure 2B). These observed differences would be consistent with a PeT effect. However, conformational heterogeneity could, in principle, also provide an explanation.

To assess the degree of rotational mobility in aqueous solution, the fluorescence emission anisotropy *r* of the freely diffusing probe molecules was measured. 1-AB, 9-AB, and 9-DAPB gave anisotropy values of 0.10, 0.05, and 0.04, respectively (Table 1). Apparently, the asymmetric attachment of the anthryl group to the BODIPY core in 1-AB results in a more hindered rotational diffusion than in the symmetric probes. Time-correlated single photon counting revealed—after correction for the instrumental response function—monoexponential fluorescence decays for 9-DAPB and 9-AB, whereas a biexponential decay was observed for 1-AB (Table 1). These measured fluorescence lifetime values are smaller than those reported for unmodified BODIPY dyes,[32] which might be attributable to alternative nonradiative pathways due to the quenching effect and rotation of the anthryl, phenyl, or sulfonate groups.

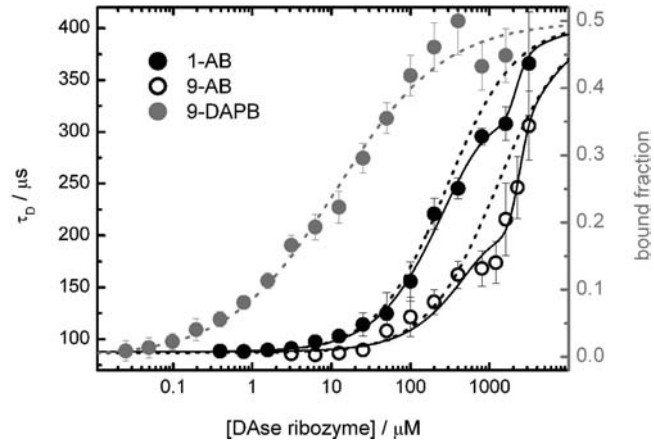

Figure 3. Determination of binding affinities of the DAse ribozyme for the probes, as measured by FCS. Diffusion times of 1-AB (left scale, black circles), 9-AB (left scale, open circles), and 9-DABP (right scale, gray circles), as a function of DAse concentration in standard DAse buffer. Solid lines represent a fit with a cooperative binding model. Dashed lines are simulated curves excluding oligomerization phenomena. Data from 9-DAPB were handled with a modified fit, in order to account for the two enantiomers (see Supporting Information).

The energy level of the BODIPY moiety is sensitively affected by the counterions of the sulfonate groups.[33] We observed substantial differences in the fluorescence intensity of the different probes as a function of salt type, concentration, and pH (see Figures S2 and S3, Supporting Information). Whereas Na^+ dramatically increases the fluorescence of 1-AB, probes 9-AB and 9-DAPB are more sensitive to K^+. The fluorescence intensity shows a counterion-dependent variation in the following order

1-AB: $H^+ > Na^+ > K^+ > Li^+ \approx Mg^{2+}$
9-AB: $H^+ > K^+ > Mg^{2+} \approx Na^+ \approx Li^+$
9-DAPB: $H^+ > K^+ > Li^+ > Mg^{2+} \approx Na^+$

Interestingly, the fluorescence of 1-AB increases with increasing NaCl concentration, the opposite behavior is found for 9-DAPB, and the 9-AB fluorescence is almost insensitive to the NaCl concentration.

Spectroscopic Properties of the Ribozyme-Bound Probes. The affinity of the Diels−Alderase ribozyme for the new probes was first investigated by fluorescence correlation spectroscopy (FCS) (Figure 3; for details, see Supporting Information).[34−36] The analysis of the autocorrelation functions revealed specific binding with K_d values of 300 ± 40, 1210 ± 190, and 12 ± 5 μM for 1-AB, 9-AB, and 9-DAPB, respectively. The values for 1-AB and 9-DAPB are in excellent agreement with the Michaelis constant K_m (370 μM) and the inhibition constant K_i (11 μM), previously determined for diene substrates and Diels−Alder products not carrying a BODIPY moiety.[13,15,17]

Binding of the probes into the hydrophobic catalytic pocket of the Diels−Alderase ribozyme was studied in the absence of the second substrate at the bulk level by absorption and fluorescence spectroscopy (Figure 4). Ribozyme concentrations

(31) Magde, D.; Rojas, G. E.; Seybold, P. G. *Photochem. Photobiol.* **1999**, *70*, 737–744.
(32) Schmitt, A.; Hinkeldey, B.; Wild, M.; Jung, G. *J. Fluoresc.* **2008**, 755–758.
(33) Shah, M.; Thangaraj, K.; Soong, M. L.; Wolford, L.; Boyer, J. H.; Politzer, I. R.; Pavlopoulos, T. G. *Heteroat. Chem.* **1990**, *1*, 389–399.
(34) Haustein, E.; Schwille, P. *Curr. Opin. Struct. Biol.* **2004**, *14*, 531–540.
(35) Lamb, D. C.; Schenk, A.; Röcker, C.; Scalfi-Happ, C.; Nienhaus, G. U. *Biophys. J.* **2000**, *79*, 1129–1138.
(36) Zemanova, L.; Schenk, A.; Valler, M. J.; Nienhaus, G. U.; Heilker, R. *Drug Discov. Today* **2003**, *8*, 1085–1093.
(37) Amirgoulova, E. V.; Groll, J.; Heyes, C. D.; Ameringer, T.; Röcker, C.; Möller, M.; Nienhaus, G. U. *ChemPhysChem* **2004**, *5*, 552–555.

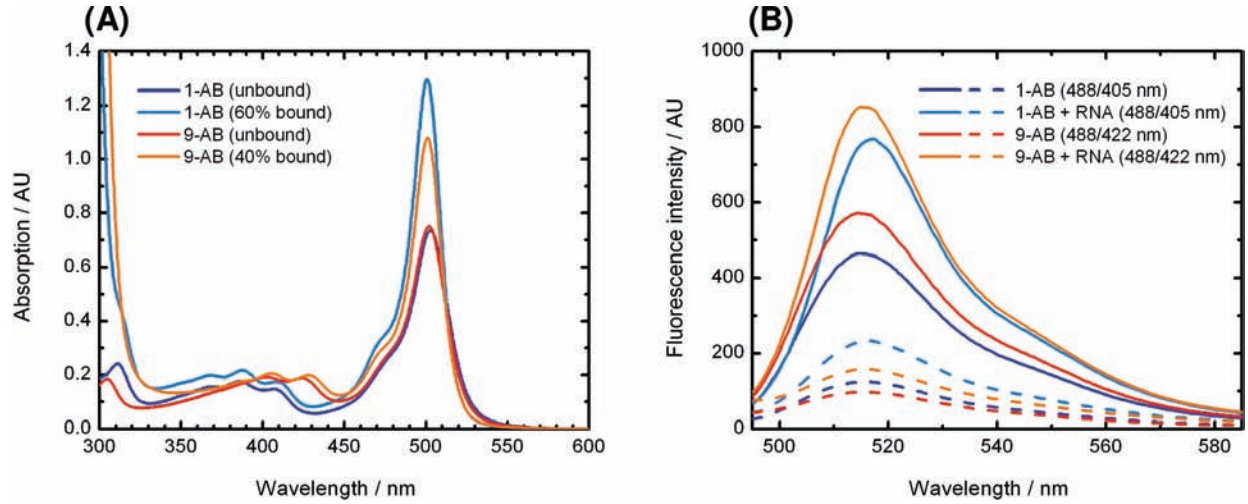

Figure 4. (A) Absorption and (B) fluorescence spectra of 1-AB (blue, 100 μM) and 9-AB (red, 100 μM) in the presence of excess ribozyme (light blue, 500 μM RNA; orange, 850 μM RNA) in standard DAse buffer. The percentage of bound molecules was calculated according to the law of mass action, using K_d values from the FCS measurements. Emission spectra with excitation at 405 or 422 nm (dashed lines) were recorded at different spectrometer settings.

were chosen so as to ensure high occupancy of the catalytic pocket. For both substrate-like probes, the relative fluorescence emission at the maximum increased significantly (+66% for 1-AB and +49% for 9-AB). For the Diels−Alder product (9-DAPB), a relative signal increase by +55% was measured (see Figure S4, Supporting Information), showing that partial quenching was still present in the unbound 9-DAPB. Considering the largely different K_d values of the probes and the fact that the measured fluorescence represents the sum of free and bound probes, measurements at different concentrations allowed extrapolation to establish the fluorescence of the bound probes only (see Figure S5B, Supporting Information). Thus, binding into the ribozyme pocket causes an increase in intensity by a factor of 2.1−2.2 for all three probes.

The absorption of the bound dyes was found to increase upon binding in a similar manner (Figure 4A and Supporting Information Figure S5A), yielding ~2.1-fold increases for the substrate-like probes and a 1.6-fold increase for the Diels−Alder product. As is evident from proportional changes in absorption and fluorescence emission, the quantum yields for 1-AB and 9-AB (0.006, 0.014) remained virtually unaffected, whereas an increase by a factor of 1.4 occurred for 9-DAPB (0.42).

The absorption spectra in the presence of RNA furthermore revealed bathochromic shifts for 1-AB (2 nm, 60% bound, 500 μM RNA) and 9-AB (4 nm, 40% bound, 850 μM RNA) of the anthracene fingers. In contrast, hypsochromic shifts of the BODIPY absorption maximum were found for 1-AB (2 nm), 9-AB (1 nm), and 9-DAPB (1 nm, 90% bound, 150 μM RNA). The decreased separation between the anthracene and BODIPY signals indicates electronic interaction between the probes and the ribozyme.

The fluorescence lifetimes of 1-AB and 9-AB were found to change only slightly upon binding to the ribozyme (see Table 1 and Supporting Information Figure S6). A strong effect, however, was seen for 9-DAPB, where the fluorescence decay was slowed from $\tau = 2.5$ to $\tau = 3.2$ ns. This retardation is consistent with the increase of quantum yield upon DAse binding. As expected for binding of a small fluorophore to a macromolecule, fluorescence emission anisotropy was increased significantly upon RNA binding (see Table 1). Anisotropy values of 0.16 (1-AB, 200 μM RNA), 0.11 (9-AB, 1200 μM RNA), and 0.20 (9-DAPB, 200 μM RNA) were measured.

To observe changes in the fluorescence intensity at the single-molecule level, we performed burst analysis measurements with a confocal fluorescence microscope.[21,37,38] In these experiments, the concentration of freely diffusing 1-AB and 9-DAPB probes was kept in the subnanomolar range as the ribozyme concentration was varied from 0 to 800 μM. Traces measured for 1-AB at ribozyme concentrations of 25 μM (Figure 5A) and 800 μM (Figure 5B) revealed that intensity bursts (the upward spikes in the traces) are much more frequent at higher RNA concentration. The histogram in Figure 5C shows intensity distributions of bursts after correction for background fluorescence and bursts from trace impurities in the RNA stock solution (which is in a 10^6-fold excess over the probe). This burst counting histogram also reveals a higher brightness of the individual bursts for 9-DAPB compared to 1-AB, consistent with their different quantum yields. Surprisingly, RNA binding does not cause an increase of the fluorescence emission from individual molecules. Rather, the frequency of bursts increases with the RNA concentration (Figure 5D and Supporting Information Figure S7). This increase agrees with the observed increase of the number of particles in the confocal volume in the FCS experiments. The observed effect suggests that the probes show a stepwise blinking behavior between on and off states. Free 1-AB is predominantly in the off state and rarely switches to the on state, which explains the low quantum yield of the molecule. For 9-DAPB, the on state is more probable. Upon binding to the ribozyme, both probes become stabilized in the on state.

The observed blinking of the probes is consistent with the assumption of photoinduced electron transfer (PeT) and corresponds well with findings from other single-molecule studies.[39,40] Photoexcitation of 1-AB and 9-AB can lead to electron transfer from the anthracene unit to the BODIPY moiety, resulting in a charge-separated nonfluorescent state. This state is expected to be stabilized through the high polarity of the surrounding medium. The fluorescence intensity of the probes depends on how efficiently the charge-separated state is depopulated, which, in turn, depends on its rotation around the phenylethynyl bridge. Because 9-AB exhibits a higher degree of conjugation than 1-AB (as seen in the UV absorption spectra, Figures 2B and 4A and Supporting Information Figure S1A), the anthracene and phenylethynyl components stay longer in the in-plane conforma-

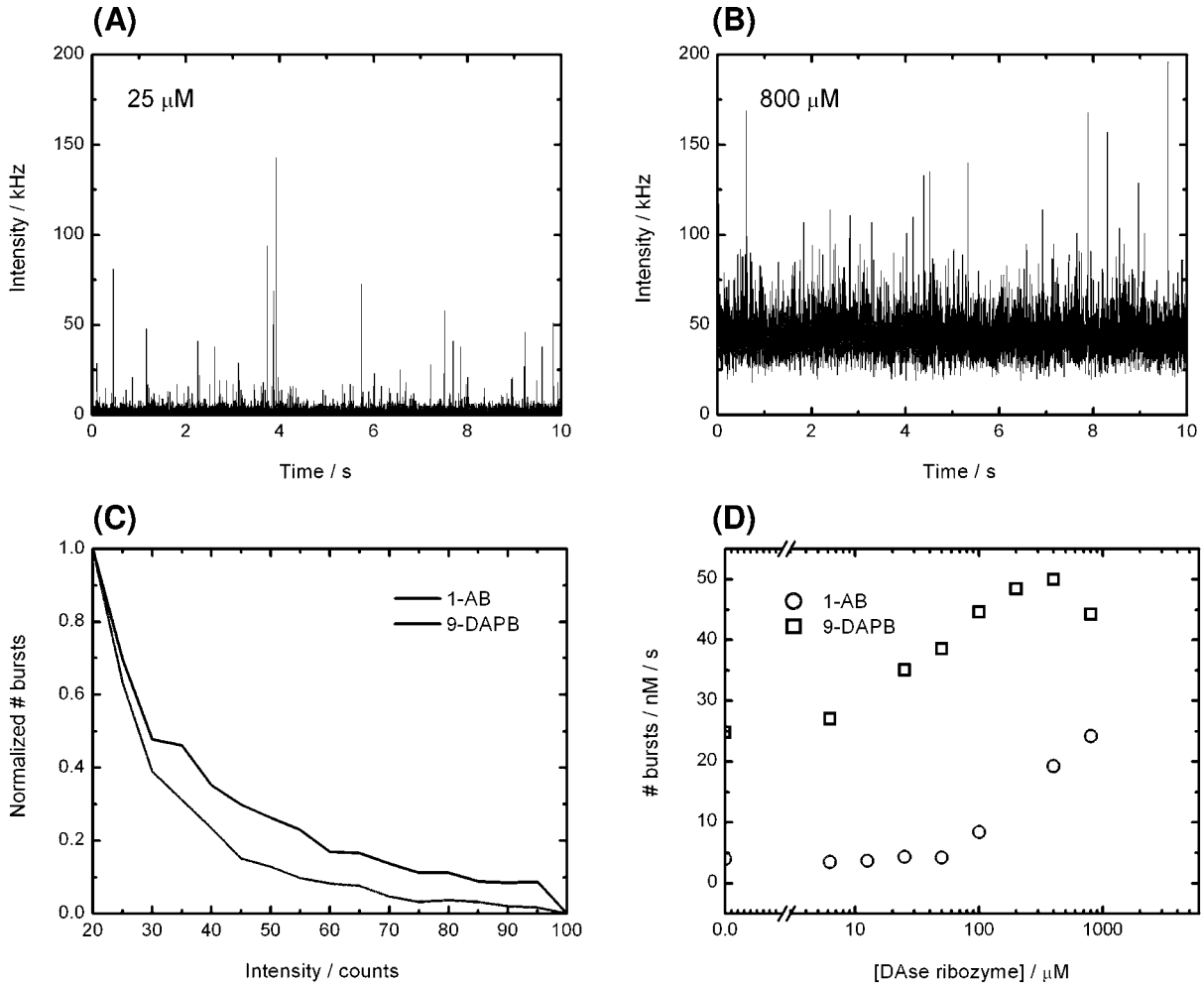

Figure 5. Single-molecule burst analysis. Ten-second fluorescence time trace of 0.25 nM 1-AB in the presence of (A) 25 and (B) 800 μM DAse ribozyme, as measured in standard DAse buffer. (C) Normalized burst counting histograms for 1-AB (gray line) and 9-DAPB (black line) taken at a DAse ribozyme concentration of 100 μM. (D) Detected number of bursts normalized to the concentration and time of measurements as a function of the DAse ribozyme concentration for 1-AB (circles) and 9-DAPB (squares).

tions, promoting charge recombination and thus higher fluorescence intensity. As a consequence, rotations around the main axis and the residence time in the in-plane states directly correlate with the blinking behavior of the probes. Further evidence supporting this model can be found in the wavelength shifts, observed in the absorption spectra at high pocket occupancies. Based on the reduction in the wavelength difference between the two subsections of the dyads, a stabilization to conformational states with higher degrees of conjugation can be deduced. Therefore, the binding process stabilizes in-plane conformations, ultimately leading to a higher blinking frequency. It should be noted, however, that the exact chemical nature of the on and off states cannot be unambiguously assigned with the data at hand.

Diels−Alderase Catalysis. The large change in quantum yield of substrate versus reaction product suggests that the increase of fluorescence upon Diels−Alder reaction can be exploited to monitor the reaction. Therefore, 1-AB and 9-AB were tested as substrates for ribozyme catalysis (Figure 6).

First, single-turnover experiments were carried out, employing a 36-fold excess of ribozyme over the anthracene component at submicromolar concentrations and the dienophile substrate at saturating concentration. A steep increase in fluorescence was observed for both probes (Figure 6A), indicating their acceptance as substrate and rapid conversion. 1-AB showed a fast reaction, reaching apparent completion within ~3 min, whereas the reaction of 9-AB was about 5 times slower. The chemical identity of the reaction products was established by HPLC (see Supporting Information). The different reactivities of the two probes likely reflect both different K_d values and stronger structural and electronic perturbations if an alkynyl-bridged substituent is attached at the 9-position, where a new bond is formed in the Diels−Alder reaction. Negative controls with the probes alone and background reactions without catalyst showed high photostability and sufficiently slow uncatalyzed reactions at room temperature.

The probes were also found to be suitable for monitoring multiple-turnover reactions. These were performed with excitation at either 488 nm (see Figure S8, Supporting Information) or 405/422 nm (1-AB and 9-AB, respectively; Figure 6B). In

(38) Kobitski, A. Y.; Nierth, A.; Hengesbach, M.; Jäschke, A.; Helm, M.; Nienhaus, G. U. *Biophys. Rev. Lett.* **2008**, *3*, 439–457.
(39) Holman, M. W.; Adams, D. M. *ChemPhysChem* **2004**, *5*, 1831–1836.
(40) Holman, M. W.; Liu, R.; Zang, L.; Yan, P.; DiBenedetto, S. A.; Bowers, R. D.; Adams, D. M. *J. Am. Chem. Soc.* **2004**, *126*, 16126–16133.
(41) Lu, H. P.; Xun, L. Y.; Xie, X. S. *Science* **1998**, *282*, 1877–1882.

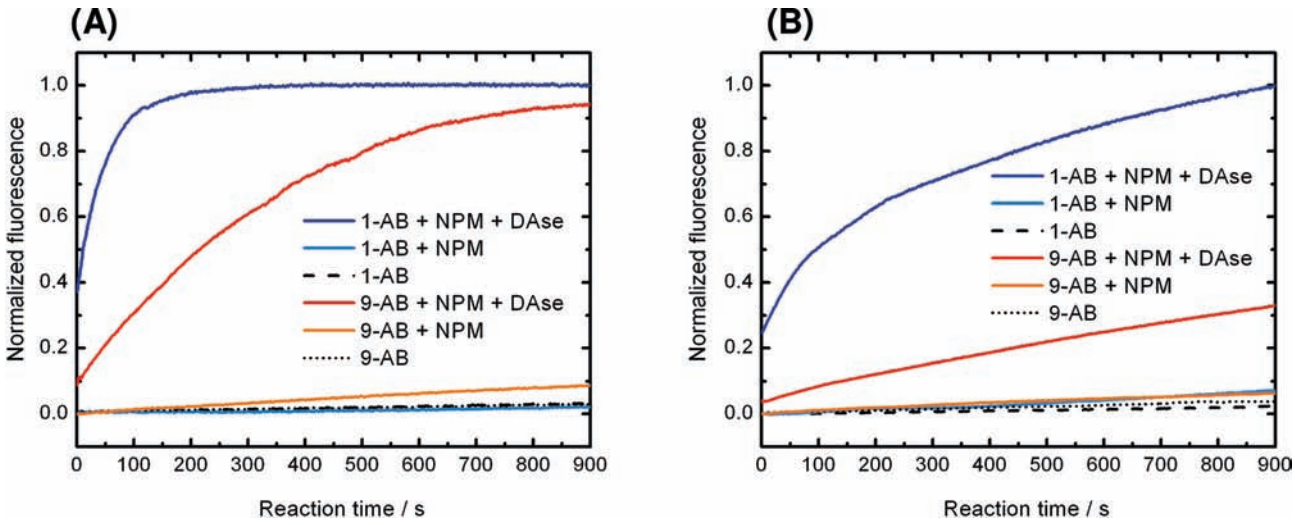

Figure 6. Fluorescence kinetics (bulk) of Diels−Alderase-catalyzed reactions at room temperature in standard DAse buffer. (A) Single-turnover conditions with 4.7 μM RNA, 500 μM *N*-pentylmaleimide (NPM), and 0.13 μM anthracene derivative 1-AB (blue) or 9-AB (red). Excitation and emission wavelengths were 488 and 515 nm, respectively. (B) Multiple-turnover conditions with 0.47 μM RNA, 500 μM NPM, and 200 μM 1-AB (blue) or 9-AB (red). Excitation and emission wavelengths were 405 nm (red, 1-AB) or 422 nm (blue, 9-AB) and 515 nm, respectively. For both experimental setups, photostability of the probes alone (dashed, 1-AB; dotted, 9-AB) and background reactions with NPM (light blue, 1-AB; orange, 9-AB) were recorded at the same conditions as for the catalyzed reactions. All experiments were started by addition of NPM 40 s prior to the fluorescence measurements.

this experimental setup, probe/ribozyme ratios up to 400:1 are possible, indicating the applicability of these probes for measuring steady-state enzyme kinetics. A quantitative comparison of apparent rate constants and the corresponding fits is shown in Figure S8 (Supporting Information).

To demonstrate the sensitivity of the molecular sensors, reactions were carried out at very low concentrations of the reactants (see Figure S9, Supporting Information). Multiple-turnover reaction kinetics of 1-AB (1 μM) with ribozyme concentrations in the 100 nM range were readily accessible.

Conclusions

Enzymatic reactions can be easily studied by fluorescence spectroscopy when the substrates or cofactors show intrinsic fluorescence.[41,42] However, the true challenge lies within systems lacking those "natural" reporters, as molecular sensors have to be specifically designed for these cases. RNA-catalyzed reactions are usually monitored using more indirect measures, in which—in RNA cleavage reactions—the distance changes between two fluorophores or a fluorophore and its quencher are followed [fluorescence resonance energy transfer (FRET) measurements].[43,44]

PeT is a well-known mechanism through which the fluorescence of a chromophore is quenched by electron transfer from a donor moiety to the acceptor. This principle was used by Urano and co-workers to design fluorescence probes for various analytes.[45] The use of the BODIPY fluorophore was reported, and the effects of various phenyl derivatives as donors (including an anthracen-9-yl) on the on/off switching of (unsulfonated) BODIPY derivatives were investigated, leading to a series of environmental polarity sensors.[3] Two of the compounds used in that study showed a marked fluorescence increase upon (unspecific) binding to a hydrophobic protein. The Burgess research group linked the BODIPY core to anthracene with structurally different linkers including phenylacetylenyl and, thereby, systematically varied the electronic coupling and the relative orientations of the two components.[23] The main focus of that work was the elucidation of the mechanism of energy transfer between the two chromophores in these energy-transfer cassettes, and strong evidence of a through-bond (as opposed to through-space) mechanism was presented.[46]

In the current study, we rationally designed molecular probes for investigating catalytic details of ribozyme-catalyzed Diels−Alder reactions that bear resemblance to these described probes. Our target compounds are water-soluble (sulfonated) BODIPY−anthracene dyads in which the BODIPY fluorescence properties are modulated by the anthracene component, consistent with the assumption of photoinduced electron transfer (PeT). We investigated specific interactions with the catalytic center of a ribozyme evolved to catalyze Diels−Alder reactions of anthracene derivatives. Despite the rather bulky modifications in comparison to the standard substrates, the probes are readily accepted and converted by the ribozyme. In particular, probe 1-AB is surprisingly well accepted and is among the best substrates ever measured for this ribozyme[17] (in terms of the ratio of the catalyzed and uncatalyzed rate constants, k_{cat}/k_{uncat}; see Figure 6).

The fluorescence properties of the probes are strongly modified by both ribozyme binding and Diels−Alder reaction. Thus, a fluorescence-based distinction of free substrate, bound substrate, bound product, and free product is possible (see Figure 7).

The unique properties of the substrate and product molecules could be employed to address specific issues concerning the catalytic cycle, including the order of substrate binding and the nature of product inhibition. Moreover, the different sensitivities for metal-ion concentration and pH value offer a wide variety of signal tuning options. Our long-term goal is the application of these probes in single-molecule experiments including (multicolor) FRET

(42) Marme, N.; Knemeyer, J. P. *Anal. Bioanal. Chem.* **2007**, *388*, 1075–1085.
(43) Ditzler, M. A.; Aleman, E. A.; Rueda, D.; Walter, N. G. *Biopolymers* **2007**, *87*, 302–316.
(44) Liu, S. X.; Bokinsky, G.; Walter, N. G.; Zhuang, X. W. *Proc. Natl. Acad. Sci. U. S. A.* **2007**, *104*, 12634–12639.
(45) Miura, T.; Urano, Y.; Tanaka, K.; Nagano, T.; Ohkubo, K.; Fukuzumi, S. *J. Am. Chem. Soc.* **2003**, *125*, 8666–8671.
(46) Kim, T. G.; Castro, J. C.; Loudet, A.; Jiao, J. G. S.; Hochstrasser, R. M.; Burgess, K.; Topp, M. R. *J. Phys. Chem. A* **2006**, *110*, 20–27.

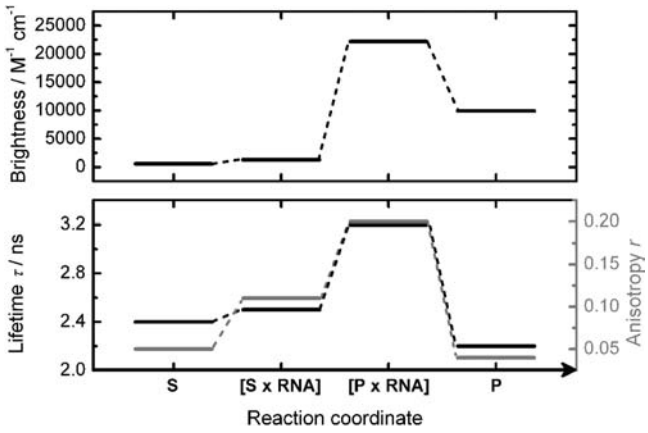

Figure 7. Variation of the 9-AB/9-DAPB fluorescence parameters of free substrate (S), bound substrate ([S × RNA]), bound product ([P × RNA]), and free product (P), arranged along the Diels−Alder reaction coordinate. Brightness was calculated as the product of the extinction coefficient at 488 nm and the quantum yield. Lifetime τ (black bars) and anisotropy r (gray bars) values are from Table 1.

to directly investigate the catalytic event and conformational changes associated with substrate binding and catalysis.[21]

Although the probes were developed for studying RNA-catalyzed reactions, the large differences in quantum yields between substrate and product probe suggests that they could find broader applications, for example, as a screening tool to find new types of catalysts for Diels−Alder reactions or other reactions that convert anthracene. Furthermore, the general construction principle of these probes, namely, the combination of BODIPY disulfonate as a fluorescence reporter and a substrate with a high electron reduction potential, might be applicable to other enzyme-catalyzed reactions.

Acknowledgment. This work was supported by the Deutsche Forschungsgemeinschaft (Ja-794-3 to A.J. and the Center for Functional Nanostructures to G.U.N.), the Volkswagen foundation (VW-I/82549 to A.J. and G.U.N.), and the Fonds der Chemischen Industrie (A.J. and G.U.N.). The authors thank Sandra Suhm for support in the synthesis and Dr. Walter Kramer for discussions of NMR spectra.

Supporting Information Available: Figures S1−S9, full experimental section, spectra of all new compounds, and complete ref 6. This material is available free of charge via the Internet at http://pubs.acs.org.

JA9084397